OPEN ACCESS

Research and educational white paper.

Not a medical device.

Correspondence

Raja Ram M*

Kryptur OU - R&D

Data Manager: Borel Sigma Data Center

Specialty section

Computational tumor metabolism and systems biology pedagogy.

Received

25 Nov 2026

Published

25 Nov 2026

Citation

Raja Ram M, Krypur Quantum R&D, Muskan S, Jain V and Swain K (2026) Metabolic Scoring Framework.

doi: 10.5281/zenodo.21873050

doi

10.5281/zenodo.21873050

ORCID icons link to author records.

Metabolic Scoring Framework

Mechanistic Scoring of Tumor Metabolic Reprogramming: A Rule-Weighted Cascade Linking Signaling, Flux, and Hallmarks

Raja Ram M [1,4*], ***Krypur Quantum R&D*** [4], ***Muskan S*** [2], ***Vipul Jain*** [3] ***and Kalinga Swain*** [3]

[1] Kryptur OU - R&D (Research & Development)

[2] Data T Research Org - Project Infrastructure

[3] AE Quantum Research Division - DCN (Digital & Cloud Networks)

[4] Zius Quantum R&D Center - Quantum & AI

Zi-us: Quantum & AI Data-T: Muskan S - Project Infrastructure Kryptur: Raja R - R&D

Keywords: Warburg effect, aerobic glycolysis, HIF-1, PI3K/Akt, Myc, p53, pseudohypoxia, PKM2, hallmarks of cancer, sensitivity analysis, computational pedagogy

Abstract

Altered energy metabolism is a defining feature of cancer, yet the logic connecting oncogenic signaling, oxygen availability, metabolic flux, and hallmark phenotypes remains difficult to teach and to reason about quantitatively. This white paper describes a transparent, rule-weighted computational framework that maps upstream inputs (oxygen, growth-factor tone, PI3K/Akt activity, Myc amplification, TP53 loss, fumarate hydratase/succinate dehydrogenase loss, and glucose supply) to HIF-1 activity, glycolytic and oxidative fluxes, a composite hallmark score, and a single phenotype score. The framework also produces interpretive biomarker proxies, concept-level attribution tables with literature links, in-silico rankings of therapeutic hypotheses, and Monte Carlo sensitivity analysis. The framework is a hypothesis generator and teaching instrument. It is not validated against patient multi-omics or clinical outcomes, it is not a medical device, and it must not be used for diagnosis, prognosis, or treatment selection.

1 Introduction

1.1 The problem

More than a century of work on tumor metabolism has produced a rich, but sprawling, literature. Students and early-career researchers must integrate oncogenic and tumor-suppressor signaling, the hypoxia response, the enzymology of glycolysis and the tricarboxylic acid (TCA) cycle, the biosynthetic demands of proliferation, and downstream consequences for the microenvironment and immune surveillance. Narrative reviews organize these layers, but do not let a learner ask counterfactual questions such as: What happens to glycolytic pressure if oxygen is restored but the PI3K/Akt axis stays active? Which metabolic node would a perturbation most affect in a hypoxic scenario versus an oncometabolite-driven scenario? How robust is any such conclusion to uncertainty in the inputs?

doi: 10.5281/zenodo.21873050

1.2 Purpose and scope

This paper documents a compact, interpretable computational framework with four design goals:

1. **Literature alignment.** Every node corresponds to a mechanism described in the primary literature, beginning with Kroemer and Pouysségur [1].
2. **Transparency.** Scores arise from rule-weighted concept attribution rather than an opaque trained model.
3. **Uncertainty awareness.** Results include Monte Carlo sensitivity analysis.
4. **Appropriate humility.** Outputs are qualitative, relative, and explicitly non-diagnostic.

1.3 What this paper is not

The framework does not predict whether a particular patient has cancer, which therapy a patient should receive, or how a tumor will respond clinically. Input parameters are abstract relative scales mapped to conceptual axes of the source literature; they are not laboratory measurements. Throughout this document, "score" denotes a mechanistic summary of a hypothetical scenario, not a measurement of real tissue.

2 Biological Background

2.1 From Warburg's observation to a modern view

In the 1920s, Warburg and colleagues reported that tumor tissue consumed glucose and produced lactate at high rates even in the presence of oxygen [2]. Warburg later argued that impaired respiration was the origin of cancer [3]. That causal claim has not survived; most tumor cells retain functional mitochondria, and mitochondrial metabolism supports biosynthesis in many tumors [4, 5]. The empirical observation remains robust: many cancer cells exhibit elevated glucose uptake and lactate secretion under aerobic conditions - the Warburg effect or aerobic glycolysis [6, 7].

Why favor a pathway that yields far less ATP per glucose than oxidative phosphorylation? Non-exclusive explanations include rapid ATP generation when substrate is abundant; diversion of glycolytic intermediates into the pentose phosphate pathway, serine/glycine biosynthesis, and lipid synthesis; and acidification of the microenvironment that may aid invasion and immunosuppression [7, 8, 9]. Critically, glycolytic flux is regulated by signaling programs that are themselves altered in cancer [1, 10].

2.2 Integrative view of Kroemer and Pouysségur

Kroemer and Pouysségur framed tumor metabolism as the intersection of signaling pathways, the metabolic fluxes they control, and the resulting hallmark phenotypes, and catalogued candidate interventions at specific metabolic nodes [1]. That layered logic - signaling to flux to phenotype to intervention - organizes the present framework.

2.3 Key regulatory nodes

Hypoxia-inducible factor 1 (HIF-1). Under low oxygen, PHD activity falls, HIF-1α is stabilized, and HIF-1 drives transcription of glucose transporters, hexokinases, LDHA, and PDK1 [11, 12]. PDK1 inhibits PDH, diverting pyruvate from mitochondrial oxidation [13, 14].

PI3K/Akt signaling. Activated Akt promotes glucose uptake and glycolytic flux and can stimulate aerobic glycolysis independently of hypoxia [15].

Myc. Myc cooperates with HIF-1 in some contexts and competes in others, regulating glycolytic enzymes, glutamine metabolism, and biosynthesis [16, 17].

TP53. p53 restrains glycolysis through TIGAR and supports oxidative phosphorylation through SCO2 [18, 19, 20]. Loss of p53 biases cells toward glycolysis.

PKM2. The M2 isoform toggles between a high-activity tetramer and a low-activity dimer; dimer bias slows the terminal glycolytic step and feeds biosynthetic branches [21].

FH and SDH. Loss causes accumulation of fumarate or succinate, which inhibit PHDs and stabilize HIF despite oxygen - pseudohypoxia [22, 23].

doi: 10.5281/zenodo.21873050

3 Framework Architecture

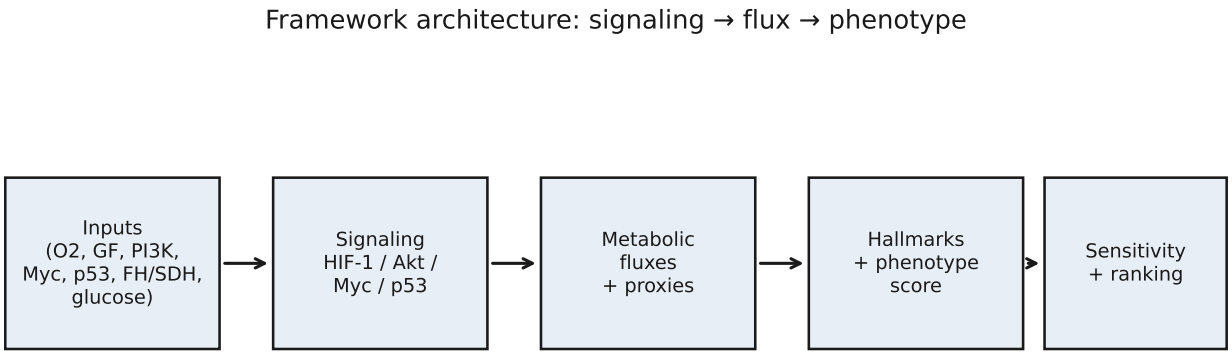

Figure 1: Framework architecture: adjustable inputs feed a signaling stage, metabolic fluxes and biomarker proxies, hallmark mapping and phenotype score, then sensitivity analysis and therapeutic-node ranking.

3.1 Overview

The framework is a feed-forward cascade with six conceptual stages (Table 1; Figure 1).

Table 1: Cascade stages and primary literature basis.

No.	Stage	Primary literature
1	O_2 / FH-SDH (PHD brake)	[11, 22, 23]
2	HIF-1 transcriptional program	[11, 12, 13]
3	PI3K-Akt-Myc integration	[15, 16, 21]
4	Glycolysis → lactate export	[6, 7, 8]
5	PDH / residual OXPHOS	[13, 14, 19]
6	Hallmark composite	[24, 25]

Each stage yields a value on a unit interval. Higher values indicate greater activity of the named process, except that OXPHOS represents residual oxidative capacity (lower values correspond to stronger glycolytic dominance).

3.2 Inputs

Seven abstract axes parameterize a scenario: tissue oxygen, growth-factor tone, PI3K/Akt oncogene drive, Myc amplification, TP53 functional loss, FH/SDH loss, and glucose availability. Literature-aligned presets include hypoxic solid-tumor-like, FH/SDH oncometabolite, PI3K/Akt-driven, TP53-loss-biased, and normoxic control cases.

3.3 Rule-weighted concept attribution

Rather than fitting parameters to a dataset, the framework assigns each concept a weight reflecting documented contribution in the source literature, combines inputs through bounded monotonic rules, and reports concept contributions to the final score. Advantages are interpretability and independence from scarce integrated multi-omic/flux data. The limitation is that weights encode expert judgment and cannot be assumed to generalize quantitatively. The approach relates to qualitative and semi-quantitative modeling traditions in systems biology [26, 27].

4 The Mechanistic Cascade in Detail

doi: 10.5281/zenodo.21873050

Concept coverage (implemented scoring nodes)

Group	Concept	Node id
metabolism	Warburg aerobic glycolysis	warburg
metabolism	Glycolysis	glycolysis
metabolism	Lactate production / MCT export	lactate
metabolism	Pentose phosphate pathway / NADPH	ppp
metabolism	PKM2 tetramer/dimer rheostat	pkm2
metabolism	Truncated TCA / acetyl-CoA export	tca_truncated
metabolism	FASN fatty-acid synthesis	fasn
metabolism	Choline kinase (ChoK)	chok
metabolism	OXPHOS / ROS / mtDNA	oxphos
clinical_readout	FDG-PET glucose uptake readout	fdg_pet
signaling	HIF-1 / PHD / VHL axis	hif1
signaling	GLUT1 glucose transporter	glut1
signaling	HK1/HK2 / VDAC coupling	hk2
signaling	LDHA	ldha

Figure 2: Concept coverage of implemented scoring nodes used to align the cascade with curated literature axes.

4.1 Stage 1: Oxygen and the oncometabolite brake

Low oxygen limits the substrate for PHD-catalyzed hydroxylation of HIF-α, while succinate or fumarate inhibit the same enzymes competitively [11, 22, 23]. The framework combines the oxygen axis and the FH/SDH-loss axis into a single PHD-activity brake.

4.2 Stage 2: HIF-1 program

HIF-1 increases glucose transport, accelerates glycolytic enzymes, and induces PDK1, suppressing PDH [11, 12, 13, 14]. PI3K-Akt-related inputs may modestly influence HIF-1, consistent with oncogene-driven HIF-1 upregulation [10, 11].

4.3 Stage 3: PI3K-Akt-Myc integration

Akt stimulates glucose uptake and hexokinase-mitochondria association; Myc upregulates glycolytic enzymes and nutrient transporters; both contribute to biosynthetic capacity [15, 16, 17]. This stage also sets PKM2 dimer bias [21].

4.4 Stage 4: Glycolysis and lactate export

Upstream drive is converted into glycolytic flux and lactate production. Lactate export through monocarboxylate transporters maintains intracellular pH and contributes to extracellular acidification [8, 9]. Export is related to, but not identical with, glycolytic flux.

4.5 Stage 5: PDH and residual OXPHOS

Residual oxidative capacity is modeled from PDH availability (suppressed by PDK1) and mitochondrial function (influenced by p53/SCO2 and oncometabolite-mediated TCA disruption) [14, 19, 22]. Higher OXPHOS argues against classic Warburg dominance [4, 5, 28].

4.6 Stage 6: Hallmark composite

Metabolic state maps to a composite of Hanahan and Weinberg hallmark capabilities [24, 25]: growth signaling, apoptosis evasion, replicative potential, angiogenesis, invasion, immune effects, and metabolism.

doi: 10.5281/zenodo.21873050

5 Biomarker Proxies

Clinicians and researchers observe tumor metabolism through limited readouts. The framework therefore derives interpretive proxy values corresponding conceptually to common assays, reported in qualitative bands and explicitly not calibrated assays (Figure 3).

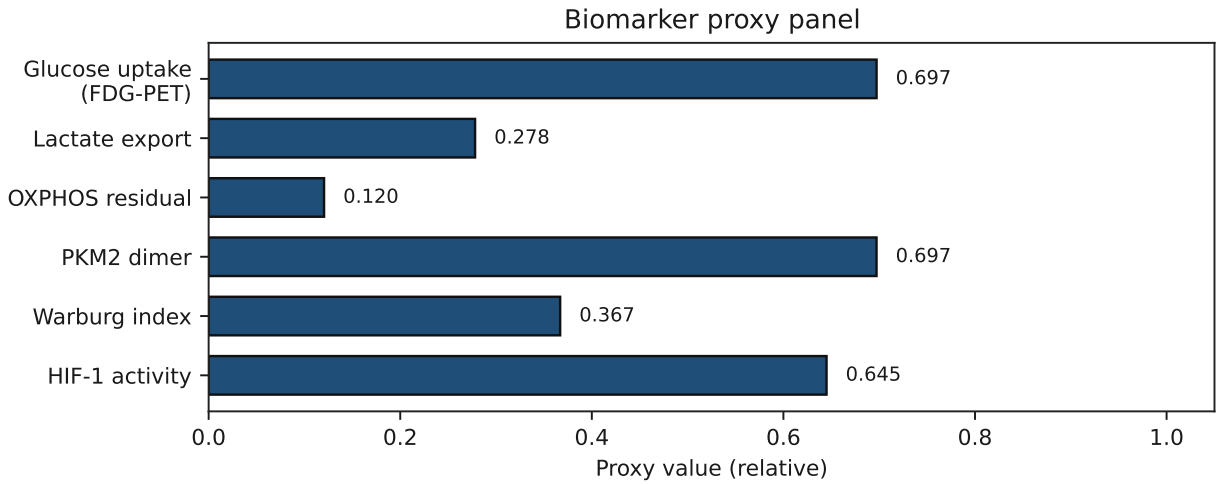

Figure 3: Biomarker proxy panel for the worked scenario (relative unit interval).

Proxies include glucose-uptake (FDG-PET-like) [29], lactate export [8, 9, 30], OXPHOS residual capacity, PKM2 dimer fraction [21], Warburg index, and HIF-1 activity [11, 22]. Proxy bands should be read together; divergence signals a mixed or transitional state [28, 31].

6 Hallmark Profile and Phenotype Score

The hallmark composite and metabolic stage values combine into a phenotype score on the unit interval. Scores may be dichotomized at 0.5 into “cancer-like” and “control-like” descriptive labels for the scenario - not predictions about a patient. Narrative verdicts accompany score bands to prevent over-interpretation of a single number. Side-by-side scenario contrast is preferred because it cancels many shared assumptions in the rule weights.

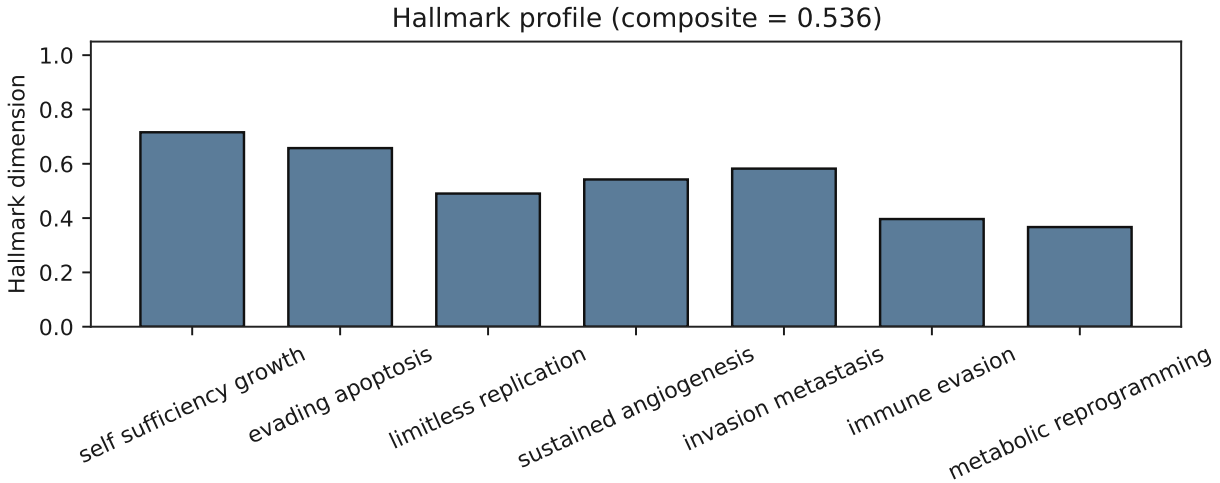

Figure 4: Hallmark dimension profile for the worked scenario.

7 Concept Attribution and Evidence Linking

For every scenario, the framework reports concepts that contributed most to the phenotype score, with contribution magnitude and curated reference pointers (Figure 5). Naming concepts rather than anonymous features lets learners

doi: 10.5281/zenodo.21873050

verify claims against primary literature and exposes single-assumption dominance [26, 32].

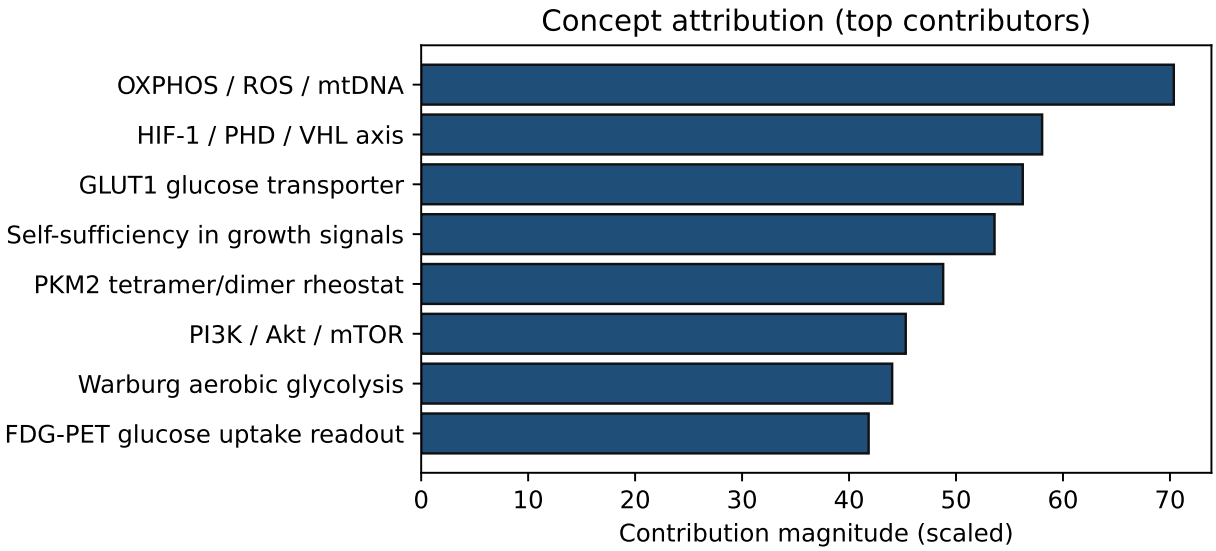

Figure 5: Top concept contributions for the worked scenario (rule-weighted attribution).

8 Therapeutic Hypotheses (Table-2 Framing)

Kroemer and Pouysségur reviewed candidate interventions at metabolic nodes [1]. The framework applies in-silico perturbations at each node and ranks candidates by change in phenotype score (Figure 6; Table 2).

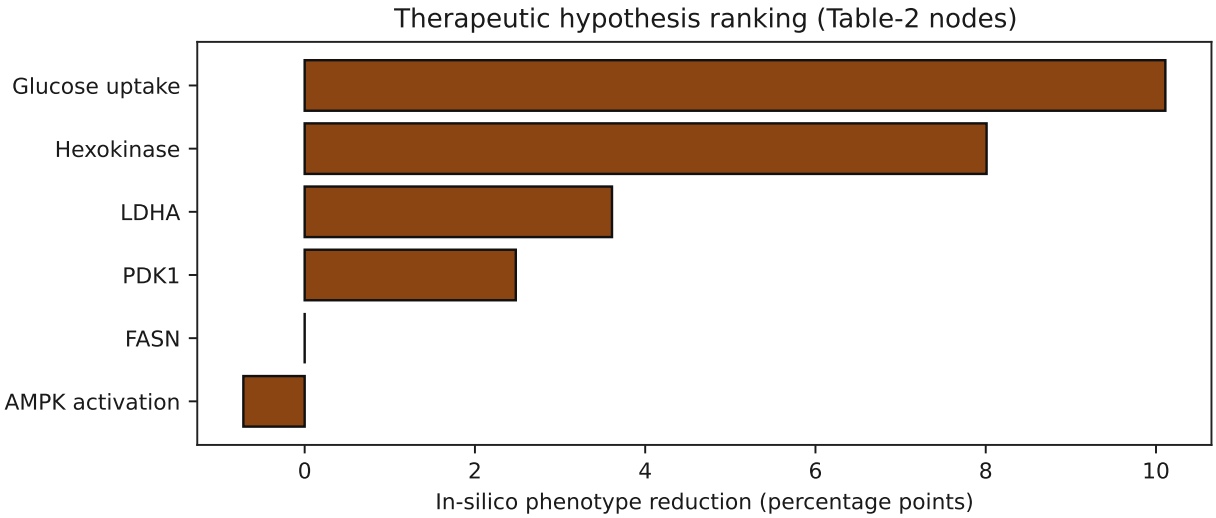

Figure 6: In-silico therapeutic hypothesis ranking by phenotype reduction (educational use only).

Upstream perturbations tend to produce larger in-silico phenotype reductions in glycolysis-dominant scenarios - a property of cascade structure, not a claim of clinical efficacy. Pharmacokinetics, toxicity, compensation, and nutrient supply are not modeled [41, 42, 43]. Rankings prioritize nodes for wet-lab or COBRA/FBA follow-up [44, 45].

9 Sensitivity and Uncertainty Analysis

Because inputs are abstract and weights reflect judgment, the framework includes Monte Carlo sensitivity analysis: input axes are sampled around set values, the cascade is re-evaluated, and the phenotype-score distribution is summarized by mean, standard deviation, and percentiles (Figure 7).

A distribution that straddles the classification threshold means the dichotomous label is unstable. Input axes can also be ranked by influence on score variance, following global sensitivity analysis logic [46, 47].

doi: 10.5281/zenodo.21873050

Table 2: Representative Table-2 metabolic nodes and agent classes.

No.	Node	Agent class	Key refs
1	GLUT / uptake & HK	2-deoxyglucose	[33]
2	HK1 / HK2	3-bromopyruvate	[34]
3	LDHA	LDHA siRNA	[35]
4	PDK	dichloroacetate	[36, 37]
5	Fatty-acid synthase	cerulenin	[38]
6	Mitochondrial complex I / AMPK	metformin class	[39, 40]

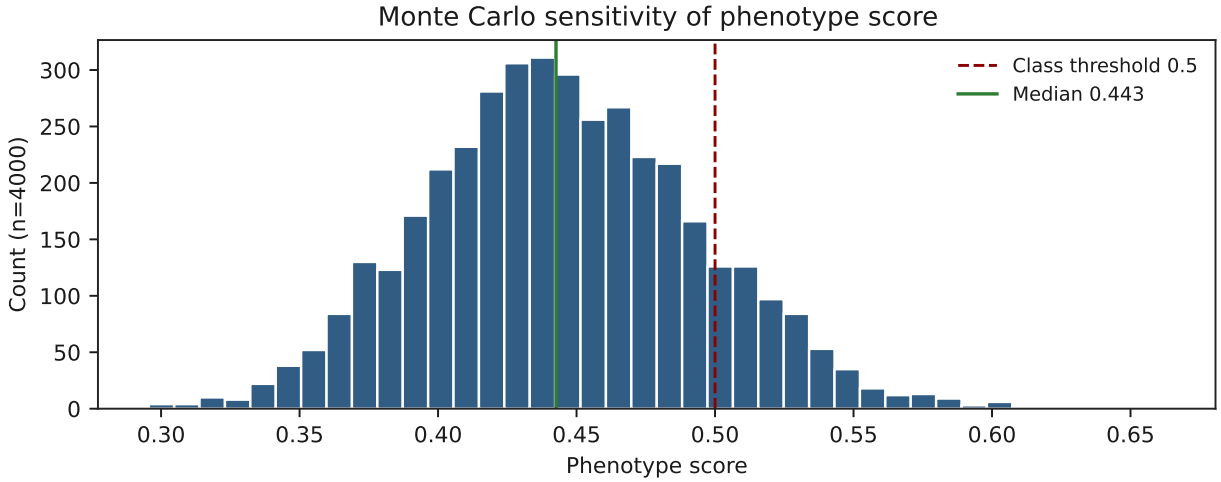

Figure 7: Monte Carlo sensitivity of phenotype score ($n = 4000$) for the worked configuration. The class threshold at 0.5 is shown for reference.

10 Worked Example

Values below illustrate framework outputs for one educational scenario and carry no clinical meaning.

10.1 Scenario setup

Tissue oxygen 0.45, growth-factor tone 0.60, PI3K/Akt drive 0.55, Myc amplification 0.50, TP53 functional loss 0.50, FH/SDH loss 0.00, glucose availability 1.00 (relative).

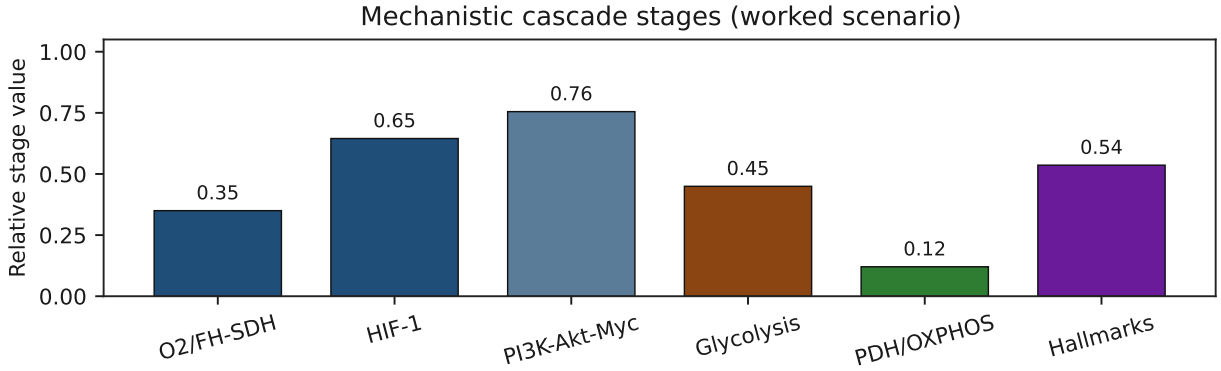

Figure 8: Cascade stage values for the worked scenario.

10.2 Phenotype and proxies

The phenotype score was 58.8% (“cancer-like” label) with a mixed/transitional narrative verdict. Biomarker proxies are summarized in Table 4.

doi: 10.5281/zenodo.21873050

Table 3: Cascade outputs for the worked scenario.

No.	Stage	Value
1	O_2 / FH-SDH brake	0.350
2	HIF-1	0.757
3	PI3K-Akt-Myc	0.912
4	Glycolysis $\rightarrow$ lactate	0.644
5	PDH / OXPHOS	0.069
6	Hallmark composite	0.647

Table 4: Biomarker proxy panel for the worked scenario.

No.	Proxy	Band	Value
1	Glucose-uptake (FDG-PET-like)	Elevated	0.924
2	Lactate export	Elevated	0.450
3	OXPHOS residual capacity	Low	0.069
4	PKM2 dimer fraction	High	0.818
5	Warburg index	Elevated	0.540
6	HIF-1 activity	High	0.757

Top concept contributions included OXPHOS/mitochondria, GLUT1 uptake, HIF-1/PHD/VHL, aerobic glycolysis, growth-signal self-sufficiency, glycolytic flux, PKM2 rheostat, and FDG-PET glucose uptake. In silico, GLUT/uptake (2-deoxyglucose), HK1/HK2 (3-bromopyruvate), and LDHA ranked highest among Table-2 nodes for phenotype reduction in this configuration. A Monte Carlo run of 4,000 samples produced a wide distribution spanning the 0.5 threshold, arguing against reporting the class label without the accompanying distribution.

11 Limitations

1. No clinical or multi-omic validation against patient outcomes.
2. Qualitative, relative units - not absolute fluxes from isotope tracing or FBA [44, 45].
3. Expert-assigned weights may misrepresent mechanisms in particular tumor types.
4. Context dependence (tissue of origin, microenvironment, heterogeneity) is omitted; glutamine metabolism, fatty-acid oxidation, and metabolic symbiosis are not modeled [5, 28, 31].
5. Hallmark mapping is coarse [24, 25].
6. Therapy ranking is not a treatment recommendation [37, 41, 42, 43].
7. Not a medical device; must not be used to diagnose, estimate prognosis, or select treatment in humans.

12 Intended Use and Governance

Appropriate uses: education; scenario comparison; hypothesis prioritization; transparent export of structured summaries for notebooks and teaching materials.

Inappropriate uses: diagnostic/prognostic interpretation; therapy selection for individuals; presenting scores as tissue measurements; claiming robustness without sensitivity analysis.

Recommended workflow: (1) select a literature-aligned scenario; (2) read the phenotype verdict as a mechanistic score; (3) inspect cascade and proxies with primary references; (4) treat intervention rankings as experimental hypotheses; (5) attach sensitivity analysis; (6) export inputs, rules, and outputs for auditability [26, 48].

13 Future Directions

Empirical calibration against public metabolic signatures and drug-sensitivity data; coupling to genome-scale reconstructions [44, 45, 49]; expanded scope (glutamine, one-carbon, lipid oxidation, redox); richer microenviron-

doi: 10.5281/zenodo.21873050

ment/immune interaction [9, 30, 50]; structured uncertainty over rule weights [46, 47]; and prospective validation with pre-specified success criteria before any use beyond education and hypothesis generation.

14 Conclusion

Tumor metabolic reprogramming is best understood as interacting layers: signaling pathways, metabolic fluxes, and hallmark phenotypes. The Metabolic Scoring Framework encodes that logic as a transparent, rule-weighted cascade with biomarker proxies, concept attribution, therapeutic-node ranking, and Monte Carlo sensitivity analysis, under explicit statements of intended use and limitation. Its value is inspectable reasoning. Its boundaries are equally important: qualitative, unvalidated against patient data, and never for diagnosis, prognosis, or treatment choice.

Author Contributions

Raja Ram M (Kryptur OU): conceptualization, methodology, software, writing - original draft, R&D leadership. **Krypur Quantum R&D / Zius Quantum R&D Center**: quantum & AI methods support. **Muskan S** (Data T Research Org): project infrastructure, data stewardship coordination. **Vipul Jain**, **Kalinga Swain** (AE Quantum Research Division / DCN): digital & cloud network infrastructure for reproducible research artifacts. **Data Manager:** Borel Sigma Data Center.

Acknowledgments

Organizational affiliations: Zius Quantum R&D Center; Data T Research Org; AE Quantum Research Division; Kryptur OU. Paper DOI: 10.5281/zenodo.21873050.

Conflict of Interest

The authors declare that this work is released for research and educational use. No clinical claims are made.

Data and Code Availability

Program source, figures, static research dashboard, and reproducible scoring artifacts accompany this manuscript in the public research repository. The interactive dashboard export is provided under `static/dashboard.html`.

Disclaimer

This document is for research and educational purposes only. It does not constitute medical advice, is not a medical device, and must not be used for diagnosis, prognosis, or treatment selection in humans. Verify bibliographic identifiers against PubMed or the publisher before formal citation.

References

[1] Kroemer G, Pouysségur J. Tumor cell metabolism: cancer's Achilles' heel. *Cancer Cell*. 2008;13(6):472-482.

[2] Warburg O, Wind F, Negelein E. The metabolism of tumors in the body. *J Gen Physiol*. 1927;8(6):519-530.

[3] Warburg O. On the origin of cancer cells. *Science*. 1956;123(3191):309-314.

[4] Zu XL, Guppy M. Cancer metabolism: facts, fantasy, and fiction. *Biochem Biophys Res Commun*. 2004;313(3):459-465.

[5] Ward PS, Thompson CB. Metabolic reprogramming: a cancer hallmark even Warburg did not anticipate. *Cancer Cell*. 2012;21(3):297-308.

[6] Vander Heiden MG, Cantley LC, Thompson CB. Understanding the Warburg effect: the metabolic requirements of cell proliferation. *Science*. 2009;324(5930):1029-1030.

doi: 10.5281/zenodo.21873050

[7] Liberti MV, Locasale JW. The Warburg effect: how does it benefit cancer cells? *Trends Biochem Sci*. 2016;41(3):211-218.

[8] Gatenby RA, Gillies RJ. Why do cancers have high aerobic glycolysis? *Nat Rev Cancer*. 2004;4(11):891-899.

[9] Fischer K, et al. Inhibitory effect of tumor cell-derived lactic acid on human T cells. *Blood*. 2007;109(9):3812-3819.

[10] Pavlova NN, Thompson CB. The emerging hallmarks of cancer metabolism. *Cell Metab*. 2016;23(1):27-47.

[11] Semenza GL. Targeting HIF-1 for cancer therapy. *Nat Rev Cancer*. 2003;3(10):721-732.

[12] Semenza GL. HIF-1: upstream and downstream of cancer metabolism. *Curr Opin Genet Dev*. 2010;20(1):51-56.

[13] Kim JW, et al. HIF-1-mediated expression of pyruvate dehydrogenase kinase. *Cell Metab*. 2006;3(3):177-185.

[14] Papandreou I, et al. HIF-1 mediates adaptation to hypoxia by actively downregulating mitochondrial oxygen consumption. *Cell Metab*. 2006;3(3):187-197.

[15] Elstrom RL, et al. Akt stimulates aerobic glycolysis in cancer cells. *Cancer Res*. 2004;64(11):3892-3899.

[16] Dang CV. MYC, metabolism, cell growth, and tumorigenesis. *Cold Spring Harb Perspect Med*. 2013;3(8):a014217.

[17] Gordan JD, Thompson CB, Simon MC. HIF and c-Myc: sibling rivals for control of cancer cell metabolism and proliferation. *Cancer Cell*. 2007;12(2):108-113.

[18] Bensaad K, et al. TIGAR, a p53-inducible regulator of glycolysis and apoptosis. *Cell*. 2006;126(1):107-120.

[19] Matoba S, et al. p53 regulates mitochondrial respiration. *Science*. 2006;312(5780):1650-1653.

[20] Jones RG, Thompson CB. Tumor suppressors and cell metabolism. *Genes Dev*. 2009;23(5):537-548.

[21] Christofk HR, et al. The M2 splice isoform of pyruvate kinase is important for cancer metabolism and tumour growth. *Nature*. 2008;452(7184):230-233.

[22] Selak MA, et al. Succinate links TCA cycle dysfunction to oncogenesis by inhibiting HIF-alpha prolyl hydroxylase. *Cancer Cell*. 2005;7(1):77-85.

[23] Isaacs JS, et al. HIF overexpression correlates with biallelic loss of fumarate hydratase in renal cancer. *Cancer Cell*. 2005;8(2):143-153.

[24] Hanahan D, Weinberg RA. The hallmarks of cancer. *Cell*. 2000;100(1):57-70.

[25] Hanahan D, Weinberg RA. Hallmarks of cancer: the next generation. *Cell*. 2011;144(5):646-674.

[26] Kitano H. Systems biology: a brief overview. *Science*. 2002;295(5560):1662-1664.

[27] Morris MK, et al. Logic-based models for the analysis of cell signaling networks. *Biochemistry*. 2010;49(15):3216-3224.

[28] Vander Heiden MG, DeBerardinis RJ. Understanding the intersections between metabolism and cancer biology. *Cell*. 2017;168(4):657-669.

[29] Gambhir SS. Molecular imaging of cancer with positron emission tomography. *Nat Rev Cancer*. 2002;2(9):683-693.

doi: 10.5281/zenodo.21873050

[30] Brand A, et al. LDHA-associated lactic acid production blunts tumor immunosurveillance. *Cell Metab*. 2016;24(5):657-671.

[31] Sonveaux P, et al. Targeting lactate-fueled respiration selectively kills hypoxic tumor cells in mice. *J Clin Invest*. 2008;118(12):3930-3942.

[32] Rudin C. Stop explaining black box machine learning models for high stakes decisions and use interpretable models instead. *Nat Mach Intell*. 2019;1(5):206-215.

[33] Pelicano H, et al. Glycolysis inhibition for anticancer treatment. *Oncogene*. 2006;25(34):4633-4646.

[34] Ko YH, et al. Advanced cancers: eradication using 3-bromopyruvate therapy. *Biochem Biophys Res Commun*. 2004;324(1):269-275.

[35] Le A, et al. Inhibition of lactate dehydrogenase A induces oxidative stress and inhibits tumor progression. *Proc Natl Acad Sci U S A*. 2010;107(5):2037-2042.

[36] Bonnet S, et al. A mitochondria-K^+ channel axis is suppressed in cancer. *Cancer Cell*. 2007;11(1):37-51.

[37] Michelakis ED, et al. Metabolic modulation of glioblastoma with dichloroacetate. *Sci Transl Med*. 2010;2(31):31ra34.

[38] Menendez JA, Lupu R. Fatty acid synthase and the lipogenic phenotype in cancer pathogenesis. *Nat Rev Cancer*. 2007;7(10):763-777.

[39] Zakikhani M, et al. Metformin is an AMP kinase-dependent growth inhibitor for breast cancer cells. *Cancer Res*. 2006;66(21):10269-10273.

[40] Wheaton WW, et al. Metformin inhibits mitochondrial complex I of cancer cells. *eLife*. 2014;3:e02242.

[41] Tennant DA, Durán RV, Gottlieb E. Targeting metabolic transformation for cancer therapy. *Nat Rev Cancer*. 2010;10(4):267-277.

[42] Vander Heiden MG. Targeting cancer metabolism: a therapeutic window opens. *Nat Rev Drug Discov*. 2011;10(9):671-684.

[43] Luengo A, Gui DY, Vander Heiden MG. Targeting metabolism for cancer therapy. *Cell Chem Biol*. 2017;24(9):1161-1180.

[44] Orth JD, Thiele I, Palsson BØ. What is flux balance analysis? *Nat Biotechnol*. 2010;28(3):245-248.

[45] Folger O, et al. Predicting selective drug targets in cancer through metabolic networks. *Mol Syst Biol*. 2011;7:501.

[46] Saltelli A, et al. *Global Sensitivity Analysis: The Primer*. Wiley; 2008.

[47] Sobol IM. Global sensitivity indices for nonlinear mathematical models and their Monte Carlo estimates. *Math Comput Simul*. 2001;55(1-3):271-280.

[48] Waltemath D, et al. Reproducible computational biology experiments with SED-ML. *BMC Syst Biol*. 2011;5:198.

[49] Agren R, et al. Identification of anticancer drugs for hepatocellular carcinoma through personalized genome-scale metabolic modeling. *Mol Syst Biol*. 2014;10:721.

[50] Chang CH, et al. Metabolic competition in the tumor microenvironment is a driver of cancer progression. *Cell*. 2015;162(6):1229-1241.

doi: 10.5281/zenodo.21873050